Chinese Chemical Letters 37 (2026) 111639

Contents lists available at ScienceDirect

Chinese Chemical Letters

journal homepage: www.elsevier.com/locate/cclet

Bromine for iodine: Unlocking short-wavelength UV phase matching in nonlinear optical metal halides

Ming-Chang Wang[a,1], Zhi Lin[a,1], Jia-Jia Li[a], Jia-Min Lian[a], Yun-Xia Hu[a], Yan Chen[b,c,*], Ke-Zhao Du[a,b,*], Jin Chen[a,b,*]

[a] Fujian Provincial Key Laboratory of Advanced Materials Oriented Chemical Engineering, Collage of Chemistry and Material Science, Fujian Normal University, Fuzhou 350007, China
[b] State Key Laboratory of Structural Chemistry, Fujian Institute of Research on the Structure of Matter, Chinese Academy of Sciences, Fuzhou 350002, China
[c] School of Environmental and Material Engineering, Yantai University, Yantai 264005, China

ARTICLE INFO

Article history:
Received 3 June 2025
Revised 14 July 2025
Accepted 25 July 2025
Available online 27 July 2025

Keywords:
OIMHs
Large SHG response
Wide bandgap
Halogen substitution
Short-wave UV phase matching

ABSTRACT

The development of high-performance nonlinear optical (NLO) crystals for the short-wave ultraviolet (UV) region remains a significant challenge. In this work, four novel organic-inorganic metal halides, $(3\text{-QUO})_2MX_4$ (3-QUO = 1-azabicyclo[2.2.2]octan-3-one; M = Zn, Cd; X = Br, I), were developed. Our initial efforts with the iodide compounds, $(3\text{-QUO})_2ZnI_4$ and $(3\text{-QUO})_2CdI_4$, yielded materials with modest second-harmonic generation (SHG) responses and, critically, they were non-phase-matchable. To overcome this, we employed a halogen-substitution strategy, replacing iodine with bromine, guided by the principle of bandgap widening. This approach successfully yielded $(3\text{-QUO})_2ZnBr_4$ and $(3\text{-QUO})_2CdBr_4$, which exhibit superior short-wave UV transparency and achieve phase-matchable SHG. Specifically, $(3\text{-QUO})_2ZnBr_4$ shows a wide bandgap of 5.10 eV (UV cutoff: 220 nm) and a phase-matchable SHG response of 1.5 times that of KH_2PO_4 (KDP). Similarly, $(3\text{-QUO})_2CdBr_4$ possesses a bandgap of 4.55 eV (UV cutoff: 245 nm) and an SHG response of 1.8 × KDP. Furthermore, these materials exhibit yellowish-white fluorescence under blue light excitation. This work demonstrates an effective approach to simultaneously tune bandgap, SHG response, and phase-matching capabilities for short-wave UV NLO applications.

© 2026 Published by Elsevier B.V. on behalf of Chinese Chemical Society and Institute of Materia Medica, Chinese Academy of Medical Sciences.

All-solid-state lasers employing second-harmonic generation (SHG) are crucial for expanding output wavelengths and achieving high-energy laser output, playing a vital role in laser frequency conversion and optical communication [1–9]. Consequently, high-performance nonlinear optical (NLO) crystals operating in the short-wave ultraviolet (UV) region (200–300 nm) have garnered significant research interest [10–13]. However, to date, only a few UV NLO crystals like KH_2PO_4 (KDP), β-BaB_2O_4 (BBO), LiB_3O_5 (LBO) have been commercialized, and these materials face a series of challenges in practical application [14–17]. Although KDP exhibits good UV transmission, its SHG response is modest ($d_{36} \approx 0.39$ pm/V) [18]. As for BBO, while pursuing strong SHG response, the birefringence of the material is often too large, especially when the π-conjugated group is the NLO active unit. The BBO crystal, based on π-conjugated $[B_3O_6]$ group is a typical example. Its large birefringence ($\Delta n \approx 0.12$@546 nm) leads to a large walk-off angle, which limits its conversion efficiency under high power conditions [19–21]. Consequently, the design and synthesis of novel short-wave UV NLO materials that simultaneously exhibit strong SHG response (>1.0 × KDP), broad ultraviolet transparency ($\lambda_{cutoff} < 300$ nm), moderate birefringence ($\Delta n = 0.05$–0.10), and high stability has emerged as a critical challenge.

Recently, organic-inorganic hybrid NLO crystals containing cyclic planar π-conjugated groups have received widespread attention from researchers [22–25]. Cyclic planar π-conjugated groups (*e.g.*, $C_5H_6NO^+$, $C_3N_3O_3^-$) typically possess large HOMO-LUMO gaps, polarization anisotropy (δ), and hyperpolarization (χ^2), rendering them classic UV NLO-active groups [26,27], with numerous high-performance NLO crystals have been reported, such as $(C_5H_6ON)(H_2PO_4)$ (3.0 × KDP, $\Delta n_{cal} = 0.25$@1064 nm) [28], $(C_7H_4NO_4)(IO_3)$ (3.6 × KDP, $\Delta n = 0.35$@546 nm) [29] and $2(C_3H_7N_6)\cdot 2Cl\cdot H_2O$ (4.3 × KDP, $\Delta n = 0.28$@546 nm) [30]. Nevertheless, despite their excellent SHG performance, the large birefringence stemming from strong π-π interactions and the substantial polarization anisotropy of organic π-conjugated rings

* Corresponding authors.
E-mail addresses: yanchen@ytu.edu.cn (Y. Chen), duke@fjnu.edu.cn (K.-Z. Du), cj2015@fjnu.edu.cn (J. Chen).
[1] These authors contributed equally to this work.

https://doi.org/10.1016/j.cclet.2025.111639
1001-8417/© 2026 Published by Elsevier B.V. on behalf of Chinese Chemical Society and Institute of Materia Medica, Chinese Academy of Medical Sciences.

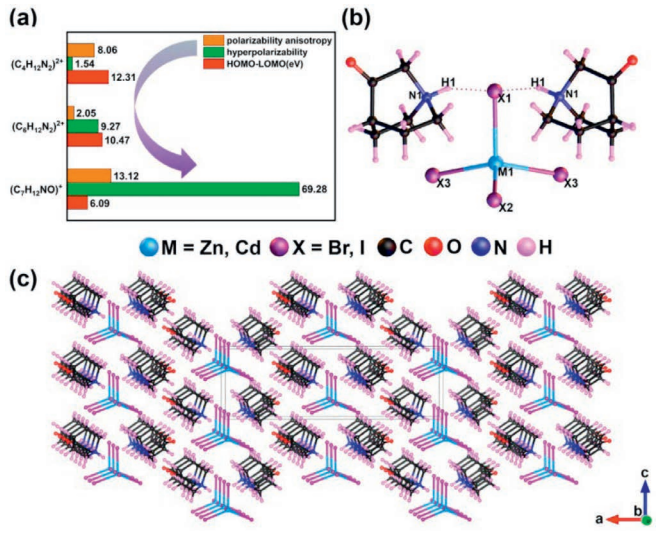


Fig. 1. The comparison of the calculated hyperpolarizability, polarizability anisotropy and the HOMO-LUMO gap of (a) the representative NLO active (non-)π-conjugated organic groups, (b) views of the $[(3\text{-QUO})_2MX_4]$ unit, (c) overall architecture of $(3\text{-QUO})_2MX_4$.

can result in excessive walk-off angles, thereby limiting their effective application. Consequently, non-π-conjugated organic groups have gained considerable interest, leading to a series of notable NLO crystals, including $[Me_3NCH_2Cl]CdCl_3$ (0.7 × KDP) [31], $H_{11}C_4N_2CdI_3$ (6.0 × KDP) [32] and (PIP)·CdI_3(HDABCO) (2.1 × KDP) [33]. Among these, 1,4-diazabicyclo[2.2.2]octane (DABCO) has aroused our interest due to its rigid bridge ring skeleton and easy growth of single crystals, and has successfully obtained a new $(H_2DABCO)CdI_4$ in the preliminary work [33]. However, the inherent small polarization anisotropy ($\delta = 2.05$) and hyperpolarization ($\chi^2 = 9.27$, Fig. S1a in Supporting information) caused by non π-conjugated $(H_2DABCO)^{2+}$ cation leads to a small birefringence (0.02@546 nm), which result in non-phase matching under 1064 nm radiation. Phase-matching (PM) requires a zero wavevector difference (Δk) between fundamental and second-harmonic waves. Typically, crystal birefringence (Δn) determined by optical anisotropy can be used to compensate for Δk and achieve PM [34–37]. Therefore, we have focused on a similar structures: 1-Azabicyclo[2.2.2]octan-3-one (3-QUO, $C_7H_{11}NO$). Compared with $(H_2DABCO)^{2+}$, $(3\text{-QUO})^+$ has a moderate HOMO-LUMO gap (6.09 eV, Fig. S1b in Supporting information), and the introduction of π-conjugated C=O groups significantly enhances polarization anisotropy ($\delta = 13.12$) and hyperpolarization ($\chi^2 = 69.28$) through electron delocalization effect, which can optimize the birefringence for phase matching under 1064 nm radiation (Fig. 1a). Moreover, the $n \rightarrow \pi^*$ transition and localized $\pi \rightarrow \pi^*$ leaps facilitate the generation of fluorescence, providing favorable conditions for the design of multifunctional optical crystals.

Following this rationale, we initially designed and synthesized a new organic-inorganic metal halide, $(3\text{-QUO})_2CdI_4$. It is speculated that it may have strong SHG response and be able to achieve phase matching under 1064 nm radiation, but the opposite is true (non-phase matching, 0.9 × KDP). Considering the strong dispersion of heavy atoms Cd and I, which may cause a red shift in the phase matching wavelength, we replaced Cd^{2+} with Zn^{2+} and successfully obtained a new isomorphic $(3\text{-QUO})_2ZnI_4$, but still exhibited non-phase matching. Nonetheless, we noticed a blue shift in its theoretical Type-I phase matching wavelength (from 544 nm to 510 nm). Previous studies have demonstrated that manipulating normal dispersion presents a viable alternative for achieving PM [34,38]. Since the refractive index demonstrates stronger frequency-dependent enhancement near the bandgap (E_g) than in off-resonance regions, normal dispersion can be reduced by enlarging E_g in NLO materials. This bandgap-widening strategy enables effective dispersion modulation to attain phase matching at shorter wavelengths. Therefore, it is reasonable to infer that halogen substitution can increase the bandgap and induce a blueshift in the PM wavelength. And we propose a halogen-substitution-mediated strategy to achieve phase matching in the ultraviolet band, resulting in a dual increase in bandgap and SHG response.

We further substituted I with Br based on the two iodine compounds synthesized previously, and successfully obtained two new $(3\text{-QUO})_2ZnBr_4$ and $(3\text{-QUO})_2CdBr_4$ which can achieve short-wave ultraviolet phase matching. Remarkably, compared to their iodide counterparts, both bromides exhibit shorter UV absorption edges and wider bandgaps ($(3\text{-QUO})_2ZnBr_4$: 220 nm, 5.10 eV; $(3\text{-QUO})_2CdBr_4$: 245 nm, 4.55 eV) as well as stronger phase-matchable SHG responses (1.5 × KDP and 1.8 × KDP, respectively). Additionally, they exhibit yellowish-white fluorescence emissions under the ultraviolet light irradiation. The fluorescence excitation peaks for both $(3\text{-QUO})_2ZnBr_4$ and $(3\text{-QUO})_2CdBr_4$ are located in the blue light region, suggesting their potential for developing single-component, blue-light-excitable white-light-emitting materials.

$(3\text{-QUO})_2MX_4$ (M = Zn, Cd; X = Br, I) has a similar structure, and all four compounds crystallize in the polar and non-centrosymmetric (NCS) space group $Pmn2_1$ (Tables S1-S5 in Supporting information). Their asymmetric units all consists of one $C_7H_{12}NO^+$ $(3\text{-QUO})^+$ cation, half of a M atom and two X atoms. In $(3\text{-QUO})^+$ cations, except for the C atom on the carbonyl group which is sp^2 hybridized, all other C and N atoms are sp^3 hybridized, and the C–C/C–N bond length and C=O bond length are consistent with the previously reported compounds (Table S3). Each M^{2+} cation is connected to four halogen atoms, forming distorted $ZnBr_4$, ZnI_4, $CdBr_4$, CdI_4 tetrahedra, and each $[MX_4]^{2-}$ anion is connected to two $(3\text{-QUO})^+$ cations through hydrogen bonds N–H···X to balance charges, forming a $[(3\text{-QUO})_2MX_4]$ unit (Fig. 1b). Neighboring $[(3\text{-QUO})_2MX_4]$ units are isolated from each other and arranged in a *quasi*-two-dimensional (*quasi*-2D) $[(3\text{-QUO})MX_4]_\infty$ layer (Fig. S2 in Supporting information), parallel to the *bc* plane. These *pseudo*-layers stack anti-parallel along the *a*-axis to form the entire 3D network (Fig. 1c).

Powder X-ray diffraction analysis (Fig. S3 in Supporting information) and the refined PXRD data (Fig. S4 in Supporting information) confirmed the purity of the synthesized samples. Field-emission scanning electron microscopy (FESEM) analyses detected the presence of C, N, O, Cd/Zn and Br/I elements in $(3\text{-QUO})_2MX_4$, the ratio of each element is consistent with structural calculations (Fig. S5 in Supporting information). The infrared spectra (Fig. S6 and Table S6) for title compounds show the C=O stretching vibration peaks around 1740 cm^{-1}, as well as the absorption peaks between 2900 cm^{-1} and 3000 cm^{-1} corresponding to N–H and C–H stretching vibrations. The peaks between 800 cm^{-1} and 1500 cm^{-1} correspond to the stretching and bending vibrations of C–C/C–N bonds on the quinine ring skeleton, with the strong peak near 1364 cm^{-1} corresponding to the C–N stretching vibration and the quinine ring skeleton vibration corresponding to the peak near 445 cm^{-1}. TG-DTA curves indicate that all four title compounds are stable up to at least 260 °C, with good thermal stability (Fig. S7 in Supporting information).

Analysis of the ultraviolet-visible (UV–vis) absorption spectra reveals a systematic variation in optical properties across the series. The absorption edge decreases in wavelength in the order: $(3\text{-QUO})_2CdI_4$ (294 nm) > $(3\text{-QUO})_2ZnI_4$ (269 nm) > $(3\text{-QUO})_2CdBr_4$ (245 nm) > $(3\text{-QUO})_2ZnBr_4$ (220 nm) (Fig. 2a). Conversely, the optical bandgap energy derived *via* Kubelka-Munk transformation increases in the order: $(3\text{-QUO})_2CdI_4$ (3.75 eV) < $(3\text{-QUO})_2ZnI_4$ (3.94 eV) < $(3\text{-QUO})_2CdBr_4$ (4.55 eV)

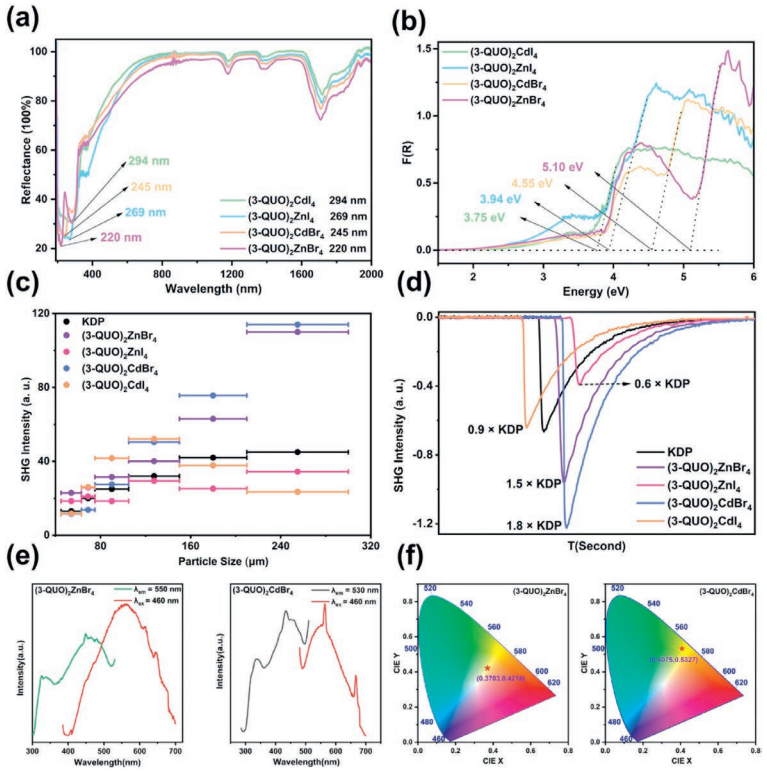


Fig. 2. (a) UV–vis diffuse reflectance spectra and (b) bandgaps for title compounds. (c) Phase-matching curves and (d) oscilloscope traces of the SHG signals (150–210 μm) with 1064 nm laser radiation. KDP was used as references for the SHG measurements. (e) The photoluminescence excitation/emission spectra of $(3\text{-QUO})_2MBr_4$ (M = Zn, Cd). (f) The CIE coordinates of $(3\text{-QUO})_2MBr_4$ (M = Zn, Cd).

< $(3\text{-QUO})_2ZnBr_4$ (5.10 eV) (Fig. 2b). This tunability, spanning the UV region from 294 nm to 220 nm (3.75–5.10 eV). The band gaps of $(3\text{-QUO})_2CdBr_4$ and $(3\text{-QUO})_2ZnBr_4$ have significant advantages over some of OIMHs containing cyclic π-conjugated organic cations, such as $C_6H_{11}N_2PbCl_3$ (3.87 eV) [39], $(C_3N_6H_7)(C_3N_6H_6)HgCl_3$ (4.40 eV) [22], $(C_6H_{10}N_2)ZnX_4{\cdot}H_2O$ (X = Cl/Br, 3.94 and 3.84 eV) [40], $(C_{13}N_3H_{14})_2MBr_4$ (M = Zn/Cd, 3.96 and 3.98 eV) [41], $(C_{10}H_{11}N_3)PbX_4$ (X = Cl/Br, 3.35 and 2.95 eV) [42]. The larger the bandgap, the shorter the UV transmission band, which is beneficial for the application of high-energy UV NLO crystals, highlights the potential values of $(3\text{-QUO})_2CdBr_4$ and $(3\text{-QUO})_2ZnBr_4$.

The SHG responses were evaluated by the Kurtz-Perry method under a laser irradiation at 1064 nm with KDP sieved as standard reference. The relationship between the SHG intensity and the particle size curve indicates the type-I phase-matchable behavior of $(3\text{-QUO})_2ZnBr_4$ and $(3\text{-QUO})_2CdBr_4$, while the non-phase-matchable behavior of $(3\text{-QUO})_2ZnI_4$ and $(3\text{-QUO})_2CdI_4$ (Fig. 2c). For $(3\text{-QUO})_2ZnI_4$ and $(3\text{-QUO})_2CdI_4$, they exhibit moderate but non-phase-matchable SHG efficiency of 0.6 times and 0.9 times that of KDP, respectively (Fig. 2d). For $(3\text{-QUO})_2ZnBr_4$ and $(3\text{-QUO})_2CdBr_4$, they achieved relatively large SHG responses at the size of 150–210 μm, which were 1.5 times and 1.8 times that of KDP, respectively (Fig. 2d). Their SHG efficiencies are superior to some of NLO crystals containing organic planar π-conjugated moieties or MX_4 tetrahedral groups, such as $(2\text{-AMP})_2BiBr_7{\cdot}H_2O$ (0.3 × KDP) [43], $(C_4H_{10}NO)PbBr_3$ (0.8 × KDP) [44], $(C_6H_5N_2)_2ZnCl_4$ (1.2 × KDP) [45], $(C_6H_{10}N_2)ZnCl_4{\cdot}H_2O$ (1.3 × KDP) [40], $(C_{13}N_3H_{14})_2ZnBr_4$ (1.12 × KDP)[41] and $(C_{13}N_3H_{14})_2CdBr_4$ (0.98 × KDP) [41].

Under UV light irradiation, all four title compounds exhibit yellowish-white fluorescence emission (Fig. S8 in Supporting information). The photoluminescence (PL) and photoluminescence excitation (PLE) spectra of $(3\text{-QUO})_2CdBr_4$ and $(3\text{-QUO})_2ZnBr_4$ were shown in Fig. 2e. Both $(3\text{-QUO})_2CdBr_4$ and $(3\text{-QUO})_2ZnBr_4$ exhibit broad emission peaks ranging from 400 nm to 700 nm, with dual PLE peaks at 440 and 330 nm. The Commission Internationale de l'Eclairage (CIE) color coordinates of $(3\text{-QUO})_2CdBr_4$ and $(3\text{-QUO})_2ZnBr_4$ are (0.4075, 0.5327) and (0.3703,0.4216), respectively (Fig. 2f). It is worth noting that the optimal excitation peaks for both $(3\text{-QUO})_2CdBr_4$ and $(3\text{-QUO})_2ZnBr_4$ are located in the blue light region. Compared with UV-light-excitable materials, blue-light-excitable materials have lower energy consumption and less damage to the encapsulant, which is significant to solid-state lighting application [46,47]. Therefore, this type of OIMH holds potential for the development of a series of single-component white-light-emitting materials excited by blue light. Meanwhile, since all four compounds can maintain good thermal stabilities (Fig. S7), which would be beneficial for their further applications.

The experimental birefringence (Δn_{exp}) of four title compounds was measured, with the single crystals in original and complete extinction states shown in Fig. 3a. As a result, the Δn_{exp} was determined to be 0.06, 0.07, 0.05 and 0.05 at 546 nm for $(3\text{-QUO})_2ZnBr_4$, $(3\text{-QUO})_2ZnI_4$, $(3\text{-QUO})_2CdBr_4$, and $(3\text{-QUO})_2CdI_4$, respectively (see Supporting information). Furthermore, to understand the phase-matching (PM) capabilities, the theoretical birefringence can be obtained *via* the calculation of the refractive index, with the values of 0.04 for $(3\text{-QUO})_2ZnBr_4$ and 0.05 for others at 546 nm, respectively (Figs. 3b-e). These theoretical values show good agreement with the experimental results. The shortest calculated wavelengths for type-I phase-matched second-harmonic generation have also been shown in Figs. 3b-e, which are approximately 405, 510, 442 and 544 nm for $(3\text{-QUO})_2ZnBr_4$, $(3\text{-QUO})_2ZnI_4$, $(3\text{-QUO})_2CdBr_4$, and $(3\text{-QUO})_2CdI_4$, respectively. Since the SHG wavelength corresponding to the 1064 nm fundamental laser used in experiments is 532 nm, these calculations predict that all four title compounds should be

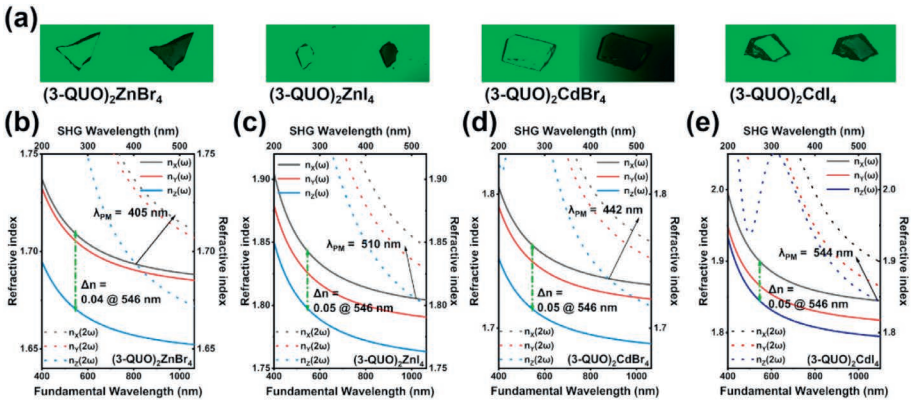


Fig. 3. (a) Original and complete extinction crystals for title compounds. Calculated birefringence and refractive index dispersion curves for fundamental and second-harmonic light of (b) $(3\text{-QUO})_2ZnBr_4$, (c) $(3\text{-QUO})_2ZnI_4$, (d) $(3\text{-QUO})_2CdBr_4$ and (e) $(3\text{-QUO})_2CdI_4$. The type-I phase matching wavelengths in different planes were evaluated based on the calculated refractive index, in which we consider the type-I phase matching condition of $n(\omega)=n(2\omega)$.

phase-matchable. However, according to the experimental results, $(3\text{-QUO})_2ZnI_4$ and $(3\text{-QUO})_2CdI_4$ exhibit non-phase-matchable behavior, which might be due to the fact that their theoretical phase-matching wavelengths have approached 532 nm. Conventional studies on isostructural OIMHs NLO crystals suggest that halogen substitution from Cl to Br to I typically yields a sequential enhancement in SHG response accompanied by bandgap narrowing, thereby limiting their operational spectral ranges [42,48,49]. Notably, in the isomorphic OIMHs systems (X = Br/I), the situation where bromides are phase-matched while iodides are not is extremely rare, as exemplified by $(MDA)Pb_2X_6$ (X = Br, I) [50]. While birefringence (Δn) conventionally compensates for Δk in crystals, its inherent optical anisotropy limits direct tunability. In this study, since the title compounds have almost the same birefringence, the bandgap widening caused by halogen substitution plays a major role in the phase matching process. This phenomenon fully validates the halogen substitution-mediated strategy, which through bromine replacement of iodine that substantially enlarges bandgaps while blue-shifting phase-matching wavelengths. This behavior originates from broader bandgaps producing flatter normal dispersion profiles, which shift the intersection point of $n(\omega)$ and $n(2\omega)$ toward shorter wavelengths (blue-shifted).

DFT calculations were employed to elucidate the origin of optical properties. It has indicated that both $(3\text{-QUO})_2ZnBr_4$ and $(3\text{-QUO})_2CdBr_4$ are indirect bandgaps, with bandgaps of 3.18 and 3.32 eV, respectively; whereas $(3\text{-QUO})_2ZnI_4$ and $(3\text{-QUO})_2CdI_4$ are direct band gaps, with bandgaps of 2.68 and 2.81 eV, respectively (Fig. S9a in Supporting information). As anticipated, these values underestimate the experimental bandgaps, a common characteristic of the GGA-PBE functional. To correct for this underestimation and better align the calculated electronic structure with experimental observations, scissor operators of 1.92 eV for $(3\text{-QUO})_2ZnBr_4$, 1.26 eV for $(3\text{-QUO})_2ZnI_4$, 1.23 eV for $(3\text{-QUO})_2CdBr_4$ and 0.94 eV for $(3\text{-QUO})_2CdI_4$ were applied, respectively. Naturally, larger experimental bandgaps necessitate larger scissor operators. Our calculations reveal a clear correlation: as the scissor operator magnitude increases, the shortest phase-matching wavelength systematically blueshifts (Fig. S10 in Supporting information). This provides a powerful theoretical insight: for an isostructural series of compounds, increasing the bandgap *via* simple elemental substitution (*e.g.*, metal or halogen tuning) directly enables a shorter phase-matching wavelength without altering the fundamental crystal packing (Fig. S11 in Supporting information). Consequently, these results theoretically validate the central innovation of our work—substituting bromine for iodine effectively yields organic-inorganic metal halides with both a wider bandgap and a more favorable phase-matching range in the short-wavelength UV region.

Additionally, the total and partial density of states (TDOS and PDOS) was conducted to clarify orbital contributions near the band edges (Fig. S9b in Supporting information). These analyses reveals distinct halogen-dependent characteristics in the band edge compositions. For bromide systems, the valence band maxima (VBM) primarily arise from Br-4p orbitals hybridized with transition metal d-states (Zn/Cd-3d) and C-2p orbitals. Conversely, the conduction band minima (CBM) in both bromides exhibit dominant contributions from C-2p and O-2p orbitals. In their iodide analogues, I-5p orbitals become the principal component of VBM alongside Zn/Cd-3d and C-2p orbitals, while the CBM maintains similar C/O-2p character as observed in the bromide counterparts. This electronic structure evolution highlights the critical role of halogen p-states in modulating VBM energetics without altering CBM orbital composition. Further confirmed that for all four compounds, both the inorganic $[MX_4]^{2-}$ tetrahedrons and the organic $(3\text{-QUO})^+$ cations synergistically contribute to the optical properties. Theoretical calculations also indicate that in $(3\text{-QUO})_2CdBr_4$, the highest occupied molecular orbital (HOMO) is primarily composed of p-orbitals from the Br atoms of the inorganic framework, while the lowest unoccupied molecular orbital (LUMO) is localized on the non-conjugated framework of the organic ligand (Fig. S12 in Supporting information). Thus, molecular orbital analysis attributes the emission to halide-to-ligand charge transfer (XLCT) [51]. The fluorescence characteristics and the HOMO-LUMO orbitals of the other three compounds are similar, and their luminescence mechanisms might be attributed to XLCT.

Due to the strong SHG responses, wide bandgaps, and phase matching of the two Br compounds, we further analyzed their SHG origins. Typically, in NLO crystals, the greater the net dipole moment, the stronger the SHG response [52,53]. Thus, we have calculated the dipole moments of the inorganic units and the net dipole moments of the unit cells using a simple bond-valence approach (Table S7 in Supporting information). The calculated dipole moment of the $[CdBr_4]^{2-}$ tetrahedron in $(3\text{-QUO})_2CdBr_4$ (4.71 D) is significantly larger than that of the $[ZnBr_4]^{2-}$ tetrahedron in $(3\text{-QUO})_2ZnBr_4$ (3.20 D). More importantly, due to the approximate crystal structure, the three-dimensional stacked $[MBr_4]$ tetrahedron (M = Cd and Zn) mainly synergistically stack along the *c*-axis direction, leading to a significant difference in the net dipole moments per unit cell: 11.31 D for $(3\text{-QUO})_2CdBr_4$ compared to 7.40 D for $(3\text{-QUO})_2ZnBr_4$, which is consistent with the experimental SHG responses. For most NLO materials, the dipole moment per unit cell normally positively correlating with the SHG intensity (*e.g.*, the net dipole moments per unit cell: 4-HPYSOF (68.36 D) and 4-APSF (11.74 D), corresponding to SHG responses of 12 and 2 × KDP, respectively [24]; S-$[Cd_2(SIAP)_2(bpy)_2]$ (9.62 D)

and S-[$Zn_2(SIAP)_2(bpy)_2$] (7.28 D), corresponding to SHG responses of 2.1 and 1.5 × KDP, respectively [54]).

In summary, we present a halogen-substitution strategy to unlock short-wavelength UV phase matching in OIMHs by replacing iodine with bromine in the $(3\text{-QUO})_2MX_4$ system. The resultant bromide compounds, $(3\text{-QUO})_2ZnBr_4$ and $(3\text{-QUO})_2CdBr_4$, exhibit significantly widened bandgaps (5.10 and 4.55 eV), blue-shifted UV absorption edges (220 nm and 245 nm), and enhanced phase-matchable SHG responses (1.5 and 1.8 × KDP), outperforming their iodide counterparts. These materials also demonstrate moderate birefringence ($\Delta n \approx 0.05$–0.06) and unique blue-light-excitable yellowish-white fluorescence, highlighting their dual functionality for nonlinear optics and solid-state lighting. This work establishes a rational approach to simultaneously optimize bandgap, SHG efficiency, and phase-matching capabilities, offering a promising pathway for designing advanced UV nonlinear optical crystals with balanced performance for next-generation photonic technologies.

CRediT authorship contribution statement

Ming-Chang Wang: Writing – original draft, Formal analysis, Data curation. **Zhi Lin:** Writing – original draft. **Jia-Jia Li:** Visualization. **Jia-Min Lian:** Visualization, Data curation. **Yun-Xia Hu:** Visualization, Data curation. **Yan Chen:** Writing – review & editing, Supervision. **Ke-Zhao Du:** Writing – review & editing, Supervision, Conceptualization. **Jin Chen:** Writing – review & editing, Conceptualization.

Declaration of competing interest

The authors declare that they have no known competing financial interests or personal relationships that could have appeared to influence the work reported in this paper.

Acknowledgments

Our work has been supported by the National Natural Science Foundation of China (Nos. 22205037 and 22373014) and the Natural Science Foundation of Fujian Province (No. 2023J01498).

Supplementary materials

Supplementary material associated with this article can be found, in the online version, at doi:10.1016/j.cclet.2025.111639.

References

[1] X. Dong, L. Huang, G. Zou, Acc. Chem. Res. 58 (2025) 150–162.
[2] P.S. Halasyamani, Nat. Photon. 17 (2023) 639–640.
[3] A.D. Poletayev, M.C. Hoffmann, J.A. Dawson, et al., Nature 625 (2024) 691–696.
[4] Y. Yang, J.W. Henke, A.S. Raja, et al., Science 383 (2024) 168–173.
[5] L. Gao, J. Chen, X. Shi, et al., Sci. Adv. 10 (2024) eadr2389.
[6] Y. Zhou, L.T. Jiang, X.M. Jiang, et al., Chin. Chem. Lett. 36 (2025) 109740.
[7] C. Hu, M. Wu, J. Han, et al., Chem. Commun. 60 (2024) 2653–2656.
[8] J.H. Wu, B. Zhang, T.K. Jiang, et al., Chin. J. Struct. Chem. 42 (2023) 100016.
[9] L. Gao, Y. Han, C. Lin, et al., Chin. Chem. Lett. 35 (2024) 109529.
[10] H. Qiu, F. Li, C. Jin, et al., Angew. Chem. Int. Ed. 63 (2024) e202316194.
[11] X. Zhou, X. Mao, P. Zhang, et al., Inorg. Chem. Front. 11 (2024) 3221–3228.
[12] H. Zhao, J. Song, S. Li, et al., Chin. Chem. Lett. 37 (2026) 111011.
[13] W. Wang, D. Mei, S. Wen, et al., Chin. Chem. Lett. 33 (2022) 2301–2315.
[14] G. Ghosh, Opt. Commun. 163 (1999) 95–102.
[15] H.T. Luo, T. Tkaczyk, E.L. Dereniak, et al., Opt. Lett. 31 (2006) 616–618.
[16] Y. Tian, W. Zeng, X. Dong, et al., Angew. Chem. Int. Ed. 63 (2024) e202409093.
[17] L.Q. Yang, X.M. Jiang, Y. Chen, et al., Adv. Opt. Mater. 12 (2024) 2301897.
[18] L. Ye, Z.L. Fang, M.Y. Guo, et al., Chin. Chem. Lett. 37 (2026) 110826.
[19] H. Qiu, F. Li, Z. Li, et al., J. Am. Chem. Soc. 145 (2023) 24401–24407.
[20] S. Wu, G. Wang, J. Xie, et al., J. Cryst. Growth 245 (2002) 84–86.
[21] J. Wang, H. Wu, Z. Hu, et al., J. Mater. Chem. C 11 (2023) 1320–1328.
[22] Z. Bai, J. Lee, H. Kim, et al., Small 19 (2023) 2301756.
[23] P. Zhang, X. Mao, X. Dong, et al., Chin. Chem. Lett. 35 (2023) 109235.
[24] L. Qi, X. Jiang, K. Duanmu, et al., J. Am. Chem. Soc. 146 (2024) 9975–9983.
[25] Y. Deng, F. Li, Z. Zhou, et al., Chin. Chem. Lett. 35 (2024) 109085.
[26] C. Shen, J. Liu, D. Sun, et al., Small 21 (2025) 2501471.
[27] C. Yang, J. Gou, Y. Zhu, et al., Angew. Chem. Int. Ed. 64 (2025) e202420810.
[28] J. Lu, X. Liu, M. Zhao, et al., J. Am. Chem. Soc. 143 (2021) 3647–3654.
[29] M.B. Xu, Q.Q. Chen, B.X. Li, et al., Chin. Chem. Lett. 36 (2025) 110513.
[30] L. Liu, C.L. Hu, Z. Bai, et al., Chem. Commun. 56 (2020) 14657–14660.
[31] C. Shen, J. Liu, K. Wu, et al., CrystEngComm 25 (2023) 2264–2270.
[32] H.Y. Wu, C.L. Hu, M.B. Xu, et al., Chem. Sci. 14 (2023) 9533–9542.
[33] M.C. Wang, M.F. Zhuo, Z. Lin, et al., J. Mater. Chem. C 13 (2025) 11651–11660.
[34] B.W. Liu, H.Y. Zeng, X.M. Jiang, et al., CCS Chem. 3 (2020) 964–973.
[35] Z. Yang, A. Tudi, B.H. Lei, et al., Sci. China Mater. 63 (2020) 1480–1488.
[36] X. Jiang, S. Luo, L. Kang, et al., ACS Photon. 2 (2015) 1183–1191.
[37] M. Mutailipu, J. Han, Z. Li, et al., Nat. Photon. 17 (2023) 694–701.
[38] M.Y. Li, X. Liu, R.X. Wang, et al., Angew. Chem. Int. Ed. 64 (2025) e202502143.
[39] Y. Kang, C. Yang, J. Zhang, et al., Chin. Chem. Lett. 37 (2026) 111385.
[40] C. Shen, C. Zhang, Q. Xing, et al., Chem. Eng. J. 509 (2025) 161389.
[41] J. Wu, Y.F. Fu, W. Liu, et al., Inorg. Chem. Front. 11 (2024) 7090–7097.
[42] L.L. Zhang, Q. Ding, P. Wang, et al., Inorg. Chem. Front. 11 (2024) 3618–3625.
[43] D. Sun, D. Wang, H. Chen, et al., Inorg. Chem. 61 (2022) 15247–15255.
[44] C. Shen, D. Sun, Y. Dang, et al., Inorg. Chem. 61 (2022) 16936–16943.
[45] D.X. Yang, Y.L. Lv, J.D. Guo, et al., Inorg. Chem. 64 (2025) 3643–3648.
[46] Y.P. Lin, S. Hu, J. Xu, et al., Chem. Eng. J. 468 (2023) 143818.
[47] Y. Zhong, Y.E. Huang, T. Deng, et al., Inorg. Chem. 60 (2021) 17357–17363.
[48] Y. Zhu, J. Gou, C. Yang, et al., Angew. Chem. Int. Ed. 64 (2025) e202509290.
[49] D. Chen, S. Hao, L. Fan, et al., Chem. Mater. 33 (2021) 8106–8111.
[50] M.A. Cassingham, Y.G. Goh, E.T. McClure, et al., ACS Appl. Mater. Interfaces 15 (2023) 18006–18011.
[51] Y. Shen, B. Wang, P. Wang, et al., Inorg. Chem. 63 (2024) 12073–12080.
[52] H. Yu, M.L. Nisbet, K.R. Poeppelmeier, J. Am. Chem. Soc. 140 (2018) 8868–8876.
[53] Y. Liu, Y.P. Gong, S. Geng, et al., Angew. Chem. Int. Ed. 61 (2022) e202208875.
[54] J. Lee, J.B. Cho, Y. Li, et al., Small 20 (2024) 2309323.